

FEATURE REMOVAL AND ISOLATION IN POTENTIAL FIELD DATA

F. Boschetti¹, V. Therond², and P. Hornby¹.

¹ CSIRO, Exploration and Mining, ARRC, 26 Dick Perry Ave, Kensington WA 6151, Australia.

² Ecole Polytechnique, route de Saclay, 91128 Palaiseau Cedex, France.

Accepted *date*. Received *date*.

Abbreviated title: Anomaly Isolation

Corresponding Author:

Fabio Boschetti

CSIRO Exploration & Mining

ARRC, Technology Park

26 Dick Perry Avenue

Kensington WA 6151

Australia

Telephone: +61 8 6436 8621

Facsimile: +61 8 6436 8555

Email: Fabio.Boschetti@csiro.au

SUMMARY

Aiming to design signal processing tools that act locally in space, upon specific features of a signal, we compare two algorithms to remove or isolate individual anomalies in potential field profiles. The first method, based on multiscale edge analysis, leaves other features in the signal relatively untouched. A second method, based on iterative lateral continuation and subtraction of anomalies, accounts for the influence of adjacent anomalies on one another. This allows to transform a potential field profile into a number of single anomaly signals. Each single anomaly can then be individually processed, which considerably simplifies applications such as inversion and signal processing.

KEY WORDS

Potential fields, Gravity, Magnetics, Signal processing, Wavelets.

1 INTRODUCTION

The analysis of one-dimensional profiles and two-dimensional images is common in many disciplines, including potential field analysis. A number of filters are available to sharpen, de-noise, or enhance the data. They are used to facilitate visual inspection by trained interpreters, or as pre-processing tools for subsequent numerical analysis. Traditionally, such filters are implemented in the Fourier domain and consequently act on all features in the signal simultaneously.

Often there is the need to remove or isolate specific features from a signal. Several tools for the inversion of potential field data, for example, work more efficiently when applied to single anomalies. Alternatively, we may want to remove large features due to known errors in the data. Clearly, such an operation would be facilitated by a representation with good spatial localisation properties, which is nevertheless directly related to the physics of potential fields.

This task is not trivial. First, we want to avoid a subjective decision on where a particular feature ends and where the adjacent feature starts. Second, we want the signal to be smooth around the selected feature. Third, we would like the selected feature to be a physically realistic potential field anomaly. Finally, we want to automate the process.

Depending on what we wish to achieve, we may or may not want to affect features adjacent to the ones we aim to manipulate. For example, to remove processing artefacts or effects due to artificial sources, we want to leave adjacent features basically untouched. In other cases, we may want to account for the influence of

anomalies on one another, as, for example, in the case of pre-processing for numerical inversion in order to reconstruct underground structures.

We describe two algorithms to address both tasks. First, we describe an algorithm in the wavelet domain that operates upon potential field signals to remove or isolate individual features, based upon the removal of multiscale edges and subsequent reconstruction. This algorithm leaves adjacent features basically untouched. A second algorithm, based on simple lateral continuation and subtractions of potential field effects, shows promising results in accounting for the effect of anomalies on one another. In this paper we show our first experiments on synthetic, noisy and real data, their results, and the directions they suggest for further work.

2 FIRST METHOD: FEATURE REMOVAL BY MULTISCALE EDGE ANALYSIS

2.1 Background to Multiscale Edge Analysis

In an introductory paper on wavelet theory, Mallat and Zhong (1992) show that the information necessary to reconstruct a signal (either a one-dimensional profile or a two-dimensional image) is contained in a subset of its wavelet transform. The magnitudes of the wavelet transform at the multiscale edges represent such a subset. Here, we briefly review the theory of wavelets and define what multiscale edges are. A more complete development can be found in Mallat and Zhong (1992).

Wavelet analysis uses two related functions to analyse a signal, a smoothing function and a ‘mother’ wavelet. The smoothing function $\theta(x)$, when convolved with the signal under study, can be viewed as an operation that removes features shorter than some characteristic length (which is a property of the function θ). To be admissible for wavelet analysis, θ must be non-negative, differentiable, and obey

$$\int_{\mathbb{R}} \theta(x) dx = 1 \quad (2.1)$$

The second function, often called “mother” wavelet function $\psi(x)$, is taken as the first derivative of the smoothing function. In one dimension,

$$\psi(x) = D_x \theta(x) \quad (2.2)$$

A signal can be analysed at multiple scales via the construction of scaled versions of θ and ψ as follows

$$\theta_s(x) = (1/s)\theta(x/s), s > 0, \quad (2.3)$$

and

$$\psi_s(x) = (1/s)\psi(x/s). \quad (2.4)$$

where s is the rescaling factor.

Given a signal $f(x)$, the wavelet transform is then defined by

$$w(s, x) = W[f](s, x) = [f * \psi_s](x), \quad (2.5)$$

where $(*)$ denotes convolution over the x domain. Then we see that

$$W[f](s, x) = [f * (sD_x \theta_s)](x) = sD_x[f * \theta_s](x) \quad (2.6)$$

which shows that the wavelet transform $W[f](s, x)$ is, except for a scale factor s , the first derivative of the signal smoothed at the scale s .

At each scale s , we define as local extrema the points at which the wavelet transform has a local maximum or a local minimum (with respect to x). The local extrema of $W[f](s, x)$ thus correspond to rapid variations in $[f * \theta_s]$, and hence can be interpreted as regions of rapidly changing intensity. In the signal processing literature these points are called ‘edges’. The collection of the edges at all scale is termed multiscale edges.

Coming to the potential field applications we address in this paper (see Hornby *et al.* (1999)), we consider the magnitude of vertical gravity acceleration f_{z_0} on a horizontal plane at height $z=z_0$ due to a density distribution ρ ,

$$f_{z_0}(x, y) = G \int_{x,y} dx' dy' \int_{-\infty}^0 \frac{\rho(x', y', z')(z_0 - z') dz'}{((x - x')^2 + (y - y')^2 + (z_0 - z')^2)^{3/2}}. \quad (2.7)$$

Here, x, y are the horizontal coordinates, G is the Newtonian gravitational constant, and the density distribution ρ is assumed zero for $z > 0$ (positive z is “up”). The Green’s function for the magnitude of vertical acceleration is

$$K(x, y, z) = \frac{z}{(x^2 + y^2 + z^2)^{3/2}}. \quad (2.8)$$

Since,

$$\int_{x,y} K(x, y, z) dx dy = 2\pi \quad (2.9)$$

for all $z > 0$, the integral of the function

$$\gamma_z(x, y) = \frac{1}{2\pi} K(x, y, z) \quad (2.10)$$

is unity for all $z > 0$. From Equations (2.9) and (2.10) and the facts that γ_z is non-negative and differentiable, we see that γ_z is admissible as a smoothing function for a wavelet, with a corresponding scaled version

$$\begin{aligned} \gamma_{sz}(x, y) &= \frac{1}{2\pi} \frac{sz}{(x^2 + y^2 + (sz)^2)^{3/2}} . \\ &= s^{-2} \gamma_z(x/s, y/s) \end{aligned} \quad (2.11)$$

Equation (2.11) the two-dimensional analogue of Equation (2.6). In analysing 1D gravity profiles it is standard practise to assume the density distribution ρ to be constant in the y direction and to integrate its effect of over y . The resulting 1D smoothing function is:

$$\begin{aligned} \gamma_{sz}(x) &= \frac{1}{2\pi} \frac{sz}{(x^2 + (sz)^2)} \\ &= s^{-1} \gamma_z(x/s) \end{aligned} \quad (2.12)$$

We define the scale $s=1$ by defining θ to be the normalised Green's function associated with some specific height z_0 , that is

$$\theta_s(x) = \gamma_{sz_0}(x) = s^{-1} \theta(x/s). \quad (2.13)$$

The corresponding 'mother' wavelet is given by:

$$\psi = D_x \theta . \quad (2.14)$$

with scaling relation:

$$\psi_s(x) = s^{-1} \psi(x/s) \quad (2.15)$$

As a result, the wavelet transform of $f_0(x)$ (the gravity acceleration at zero height) is given by

$$\begin{aligned} W[f_0](s, x) &= [f_0 * \psi_s](x) \\ &= s D_x [f_0 * \gamma_{sz_0}] \\ &= (z/z_0) D_x f_z(x) \end{aligned} \quad (2.16)$$

where $s = z/z_0$.

The wavelet transform of the gravity profiles can thus be calculated at scales $s > 1$ from measurements at height $z = z_0$ as follows:

- 1) Upward continue the measured profile to a level $z = sz_0$,
- 2) take the gradient of the profile along x and
- 3) multiply the resulting profile by the factor $s = z/z_0$.

No new processing software is needed to calculate these wavelet transforms since the operations listed above are part of the standard tools for any potential field practitioner.

At this point, remembering that the collection of edges at all scales of the wavelet transform is named the multiscale edges, all is left to do is to pick the multiscale edges at the location where the wavelet transform has a local maximum or minimum.

Thus, a point i along a profile is defined a edge if

$$f_{i-1} < f_i \text{ and } f_{i+1} < f_i \quad \text{or} \quad f_{i-1} > f_i \text{ and } f_{i+1} > f_i$$

For one-dimensional profiles the multiscale edges group themselves into strings in the scale-space wavelet domain. Their positions and shapes are strongly related to the

locations and shapes of individual features in the profile. This provides a visually intuitive representation of the signal and of the relation between features within the signal at different scales. As an example, in Fig. 1 we show a gravity profile (top) and its multiscale edges (middle). The edges form strings that arise from the major anomalies in the profile. In the wavelet literature these strings are called branches, whilst the collection of branches is called an edge tree. The correspondence between features in the profile and edge branches is due to the localisation property of wavelets. This suggests that by manipulating *some* edge branches and reconstructing the profile, the features corresponding to such branches could be modified, thus allowing a signal processing tool to operate locally on specific parts of the image, leaving the rest minimally perturbed.

Mallat and Zhong (1992) tested the idea for noise suppression applications. They discriminated between branches due to noise and branches due to main features in an image by studying their behaviour at different scales, and suppressed the former ones before reconstructing the signal. Lu et al. (1994) employed the same idea by artificially amplifying the magnitude of the edge branches before image reconstruction. In this way they obtained much sharper features in medical images.

In this work, we extend such results. Our application differs from noise removal since the features we attempt to remove are of large magnitude and spatial extent. Unlike high-frequency noise, the edges of large features exist at a large number of scales. Also, unlike the application by Lu et al. (1994), we try to remove (and consequently to manipulate the edges of) individual features only. This generates distortion in the wavelet representation that needs to be treated with care.

2.2 Reconstruction Algorithm from Multiscale Edges

The crucial part in the design of multiscale-edge-based signal processing is the algorithm that reconstructs the signal from its multiscale edges. The process of going from a signal to its edge tree and back can be seen as a mathematical transform in itself, much like a Fourier or wavelet transform. For the sake of clarity we will call this transform a Multiscale Edge Transform (MET), as opposed to the standard Wavelet Transform (WT). A discussion of the accuracy of the MET and its computational cost can be found in Mallat and Zhong (1992) and Mallat (1998).

The MET itself requires the intermediate step of a traditional WT as summarised in Fig. 2. The first step builds the WT of the signal using upward continuation and differentiation. From the WT we extract the multiscale edges as local extrema of the WT. These two steps have been described above in details. This represents the forward MET. In the inverse MET we first reconstruct a proper WT from the multiscale edges and then perform an inverse WT to go back to the signal. The crucial part of the inverse MET relevant to this paper is the algorithm that reconstructs the WT of a signal from the MET of the signal.

In Mallat and Zhong (1992), this is achieved by requiring that the WT be simultaneously in two subsets, namely:

- 1) the set of scale-space functions having extrema only at the multiscale edges and wavelet magnitudes equal to those on the multiscale edges – P_1 is the operator that maps any scale-space function into this set;

2) the space of all possible wavelet transforms – P_2 is the projection onto this subspace of scale-space functions.

The reconstruction from multiscale edges is usually achieved by iterating the application of the two operators (P_2P_1) to some initial guess.

The projection P_2 is achieved by passing a candidate scale-space function through the reproducing kernel. This consists of an inverse WT followed by a forward WT. Being an orthogonal projection, the reproducing kernel operator produces the element of the space of possible WT functions that is closest to the candidate scale-space function it acted upon (e.g. Kaiser 1994, p87; Hornby et al, 1999, p195).

Unfortunately, operator P_1 is not so easily represented by a straightforward projection operator due to the non-convex nature of the constraints represented by the multiscale edges. It is instead approximated by monotonically interpolating between the multiscale edges along the x-direction (see Lu, 1997, p. 18). Such an interpolation over x is applied independently at each scale. We call the result of such operator $\hat{w}(s,x)$. In the iterative process $\hat{w}(s,x)$ is taken as a candidate for the ‘correct’ WT $w(s,x)$. The WT reproducing kernel projection P_2 is then applied to $\hat{w}(s,x)$ to create a function that is closest to $\hat{w}(s,x)$ within the set of ‘correct’ WT.

In practice, P_1 is constructed through a series of three operators:

- sampling (P_S),
- monotonic interpolation between edges (P_I) and
- "wiggle removal" (P_M).

Let's define as $\{x_i^s\}$ the x position of the edge i ($i = 1 \dots N$, where N is the number of edges at scale s) at scale s . P_I is an interpolator that interpolates monotonically over x in each interval $[x_i^s, x_{i+1}^s)$ between two consecutive multiscale edges. (Notice that the interval $[x_i^s, x_{i+1}^s)$ is written with two different brackets, because we assume x_{i+1}^s to belong to the 'next' interval). P_S represents the operation of sampling the values of a function of scale-space at the multiscale edges $\{x_i^s\}$. The third operator P_M is defined in each x-interval $[x_i^s, x_{i+1}^s)$ by

$$P_M[w](s, x) = \begin{cases} \max\{\inf_{x_i^s \leq t < x} \{w(s, t)\}, w(s, x_{i+1}^s)\} & \text{for } w(s, x_i^s) \geq w(s, x_{i+1}^s) \\ \min\{\sup_{x_i^s \leq t < x} \{w(s, t)\}, w(s, x_{i+1}^s)\} & \text{for } w(s, x_i^s) \leq w(s, x_{i+1}^s) \end{cases} \quad (2.17)$$

which is applied independently at each scale s . The operation P_M removes wiggles from the intervals $[x_i^s, x_{i+1}^s)$ by replacing "humps" or "dips" in the graph of $\hat{w}(s, x)$ (the current best estimate of the 'correct' $w(s, x)$) by straight horizontal lines, yielding a function $P_M \hat{w}(s, x)$ that is monotonic over x for all the intervals between multiscale edges. We now have all the elements required for our iteration scheme. This can be described as follows:

- 1) given $w = w(s, x)$ as the actual wavelet transform, generate the MET we wish to invert as $P_S w$, which represents the wavelet transform sampled at the positions $\{x_i^s\}$ of the multiscale edges.
- 2) Interpolate $P_S w$ monotonically over x , by applying $P_I P_S w = P_{SI} w$

- 3) project this into the set of wavelet transforms to obtain our first approximation $\hat{w}(s, x)$ to w by performing $P_2 P_{SI} w$. This function may now suffer two inconsistencies. It may neither have the correct value at the multiscale edges, nor be x-monotonic between multiscale edges. Consequently:
- 4) force agreement between the values of $\hat{w}(s, x)$ and w at the multiscale edges by a) sampling the current approximation ($P_2 P_{SI} w$) at the multiscale edges using P_S , b) subtracting these sample values from the actual MET values (w), c) interpolating the differences monotonically, and d) adding the P_I interpolated difference back to $P_2 P_{SI} w$.
- 5) Finally, enforce monotonicity over x between edges by acting on this corrected approximation with P_M . We now have a new function that matches the values at the multiscale edges and is monotonic between them.
- 6) act again upon P_2 to form the next approximation to w .

This defines the iterative scheme

$$\begin{aligned}
w^{n+1} &= P_2 P_M \left(w^n + P_I \left(P_S w - P_S w^n \right) \right) \\
&= P_2 P_M \left(w^n + P_{SI} \left(w - w^n \right) \right)
\end{aligned} \tag{2.18}$$

where $w^0 = 0$. Substituting the actual WT $w = w(s, x)$ into Equation (2.18) yields the self consistency requirement $w = P_2 P_M w$, which is indeed the case because $w = P_M w$ by construction of P_M , and the fact that P_2 is the reproducing operator for the WT. Defining the error by $e^n = w - w^n$, one finds that the errors obey

$$e^{n+1} = P_2(P_M w - P_M(w^n + P_{St}e^n)), \quad (2.19)$$

which does not necessarily simplify further due to the non-linearity of P_M .

The MET inversion algorithm has been well tested and good results are reported in the literature (see, for example, Lu et al., 1994). Our own experience suggests the algorithm be stable and robust. Usually a satisfactory reconstruction is achieved within 20 iterations. An example of the quality of reconstruction can be seen in Fig. 1. The top plate shows a synthetic gravity profile. The bottom frame shows the profile reconstructed using only the edges shown in the middle plate. The two profiles are basically identical. Our next step is to test the effectiveness of the MET as a tool for signal processing.

2.3 Feature Removal

We apply the algorithm presented in the above section to the removal of an individual anomaly in the gravity profile in Fig. 3a. In Fig. 3b we can see the edge tree. We want to remove the anomaly on the left. In order to do so, we remove the edge branches on the left, which correspond to the left anomaly. The remaining edge tree is presented in Fig. 3c. The result after reconstructing the profile is shown in Fig. 3d. We can see that the left anomaly is not completely removed. A small bump remains in the profile. We will discuss the reason for this and suggest an improvement later. For the moment we note that the magnitude of the remaining bump is quite small considering the rather brutal nature of the edge manipulation.

Fig. 3e shows the difference between the profiles in Figs 3a and 3d. We can see the isolation of the anomaly on the left. Most importantly, we see that in place of the anomaly on the right only minor oscillations occur. This shows that the right anomaly has been left almost untouched by the process. Depending on the purpose of the processing, this may or may not be entirely desirable, as we shall subsequently point out.

It should be emphasised once more that a similar result would not be possible with traditional signal processing in the Fourier domain. Any filter applied to one anomaly would act in the same fashion on any other anomaly in the profile. This approach also has advantages when compared to manual isolation. First, we avoid a subjective judgement of where one anomaly ends and where the adjacent one starts. Second, the algorithm implicitly imposes smoothness in the profile, by suppressing spurious edges.

3 SECOND METHOD: FEATURE REMOVAL BY LATERAL CONTINUATION

In the previous section we showed how the multiscale edge method allows the removal of one anomaly from the profile while leaving the adjacent anomaly basically untouched. This feature could be beneficial for a number of image processing applications, such as the removal of artefacts or of responses due to artificial sources. If, however, we aim to remove the response of a natural source, then we may be interested in also removing the influence that such a source has on adjacent features. Basically, we may want to reconstruct the remaining profile as if

the source generating the anomaly to be removed was not present. We illustrate this process next. Before we do that, we should notice that the classic ambiguity inherent in potential field studies does not allow a unique solution for such a problem. In this work, we assume that causative sources are simple ‘Euclidean shapes’ of constant density.

Let us suppose that we want to remove the leftmost feature of the signal in Fig. 4a (this is the same signal we used in the test of the MET method). The method that we propose can be summarised in three steps.

- 1) Continue the right hand side anomaly laterally to the left as if the left anomaly was not present (Fig. 4b), (details on how to continue the anomaly laterally are given next) and then subtract this approximation from the original signal. The result can be seen in Fig. 4c. This represents our first guess at the reconstruction of the left hand side anomaly.

- 2) Continue the left anomaly laterally to the right (Fig. 4d). This step is necessary in order to account for the correct value of the anomaly edges by approximating the right flank of the left hand side anomaly (see below). Subtract this approximation from the original signal (Fig. 4e). This represents our first guess at the reconstruction of the right hand side anomaly.

- 3) Iterate steps 1 and 2 until the difference between the profiles obtained at the end of two consecutive iterations falls below a certain threshold.

The rationale of the algorithm is that, at each iteration, part of the effect of one anomaly is removed from the adjacent one. This, in turn, allows for a better approximation of the anomaly itself, and consequently a more accurate lateral extension at the next iteration. This proceeds until convergence is reached. For nicely separated anomalies, as in this example, 3-5 iterations suffice. In more complicated cases we may want to perform a few tens iterations.

Clearly, the crucial element of this algorithm is the lateral continuation of the anomaly. We choose to approximate this part of the profile by the gravity response to a point source. The reason can be explained with the help of Fig. 5. Despite the ‘real’ source generating the profile is spatially extended (rectangular block in Fig. 5b), a point source, laterally displaced from the centroid of the block, gives a reasonable approximation of the left-hand side of the profile (thick line).

The gravity response of a point source can be written as:

$$f(x) = \frac{hm}{(x-c)^2 + h^2} \quad (3.1)$$

where c is the horizontal position of the point source, h its depth, and m is its mass. Returning to the example in Fig. 4, we calculate the three parameters c , h , and m , for the extrapolation of the left flank of the right hand side anomaly, using three points along the profile (see Fig. 6). The first point is the barycentre of the two edges involved: the right edge of the left anomaly and the left edge of the central anomaly. Each edge is given a weight proportional to the width of the anomaly it belongs to. The width of the anomaly is approximated by the spacing between its edges at the finest scale. The third point is the edge of the main feature (right hand side anomaly in this case), and the second point lies in between the first and third points.

This results in the following analytical formulae to calculate the three parameters c , h and m , from the points (x_1, y_1) , (x_2, y_2) , (x_3, y_3) :

$$c = \frac{1}{2} \cdot \frac{x_1^2 y_1 (y_2 - y_3) + x_2^2 y_2 (y_3 - y_1) + x_3^2 y_3 (y_1 - y_2)}{x_1 y_1 (y_2 - y_3) + x_2 y_2 (y_3 - y_1) + x_3 y_3 (y_1 - y_2)} \quad (3.2)$$

$$h = \sqrt{\frac{y_2 (x_2 - c)^2 - y_1 (x_1 - c)^2}{y_1 - y_2}} \quad (3.3)$$

$$m = \frac{y_1 ((x_1 - c)^2 + h^2)}{h} \quad (3.4)$$

The final result of the separation of the anomalies in Fig. 4 is illustrated in Fig. 7. Figs 7b and 7c show the right hand side and left hand side anomalies, respectively, after separation. For ease of comparison Fig. 7a shows again the original anomaly.

In order to be useful, the algorithm needs to reconstruct a good approximation of the ‘true’ anomaly, (that is of the anomaly as if the source generating the anomaly to be removed was not present), and be robust to noise. Fig. 8a shows the same anomaly used in the test in Fig. 1, to which a considerable amount of noise has been added. We used a random white noise whose maximum amplitude is 15% of the signal amplitude. In the Figure, the dashed lines show the noisy signal, the thick lines show the signals after removal of the left hand side anomaly and the dotted lines show the noise-free ‘true’ signal due to the source which generated the right hand side anomaly. As can be seen from Fig. 8a, the isolated and true anomalies are hardly

distinguishable. In Figs 8b-d we show the same test case, in which the sources generating the two anomalies are brought progressively closer, resulting in stronger anomaly interference. Departure between ‘true’ and reconstructed signal is noticeable only in the last frame (8d), when the anomalies are very close. We believe that a more sophisticated method than a single point source to reconstruct the flank of the main anomaly could improve the performance of the algorithm in this situation, as will be discussed later.

The algorithm robustness to noise is not surprising. First, the anomaly is extended laterally accounting mostly for the information contained in the signal edges. These are the most stable points in the profile (see Hornby et al, 1999). Secondly, the lateral extension is the result of a point source approximation, which also is little affected by the signal noise.

4 AUTOMATING THE ALGORITHMS

A crucial feature of both algorithms is that they can be easily automated. This not only makes their use simple and fast, but also removes any subjectivity in choosing where the anomalies should be separated. The key to the automatization lies in the concept of edge and in its unique relation to the main anomalies in a signal.

Once an anomaly is chosen (by selecting a point close to its peak, for example), simple edge detection algorithms can easily determine the edges of the corresponding anomaly. The successive steps differ for the two algorithms:

- 1) in the case of the MET, we need to follow the edge branches arising from the two edges of the anomaly, and remove them completely. Following the edge branches is easy to implement since they follow a continuous curve in scale space.
- 2) In the case of the lateral continuation algorithm, we simply need to determine the adjacent anomaly from which the current anomaly needs to be removed. This simply implies progressing along the profile until a new set of edges is found.

In case of noisy profiles, several edges may arise from the same anomaly at small wavelet scales. This problem can easily be circumvented by looking at the edges at a coarser scale (at which all noise induced edges have died out) and then follow the corresponding edge branches backward.

5 DISCUSSION

Multiscale edge-based signal processing works by manipulating some branches in the edge tree and reconstructing the signal from the modified MET. In our applications we have generally removed edge branches completely. When we do this, we distort the MET. It is true that the value of the MET at a given edge point and given scale contains mainly information about features within a spatial region of approximately that scale surrounding that edge point. However, since our Green's function-based wavelets are not completely local, edge points also contain some information about more distant features. When we delete some edge branches in an attempt to remove

the corresponding features, some of the information about those features persists in surrounding edge branches that we do not remove. This is especially true of remaining edge points that are close to a removed edge point, where "close" is relative to the scale of the edge point being removed. When we try to reconstruct a WT from the distorted MET, the reproducing kernel operator P_2 tends to re-insert edge features (at reduced amplitude) near the location where we tried to eliminate them.

Re-establishing x-monotonicity between edges through the inclusion of P_M generally works very well in inverting an exact MET. However, the algorithm cannot always eliminate oscillations arising from a pseudo-MET distorted by edge removal. The problem arises through the fact that $(P_M - P_2 P_M)w^n = (1 - P_2)P_M w^n$ does not approach zero. In this case P_M continues to remove oscillations, and P_2 continues to replace them. One possible solution is to avoid exactly fitting the remaining edges in the distorted MET. We should instead use the distorted MET as a prior hypothesis on the edges, and allow this to compete with the monotonicity and WT properties expressed by P_M and P_2 respectively. Moreover, in the feature isolation application, we should also include constraints on the asymptotics and edge content of both the isolated feature and residual profiles. In this way we might achieve the unmixing of physically realisable signals.

In our opinion, the results we have presented for MET filtering are analogous to poorly-applied Fourier analysis using abrupt filters and no tapering or padding of the data. Attention to filter design and data preparation mitigate the well-known artefacts of poorly-applied Fourier processing. We feel that with a better understanding of

MET processing, the artefacts created by the MET filters presented here can be similarly tamed.

Improvements can also be achieved in the iterative method via lateral continuation. One avenue involves taking advantage of potential field non-uniqueness in order to generate sources that are better able to model the anomalies than the point source employed in this study. Then, by removing such ‘ad hoc’ source models, we may improve the anomaly isolation.

5.1 Applications

In the following we show two potential applications of the algorithm to inversion and signal processing. In both cases we show the benefit of analysing each individual anomaly separately against the single analysis of the overall profile. In both cases we aim at isolating anomalies by also removing the effect of adjacent anomalies. Consequently the algorithm involving lateral continuation will be used.

5.2 Inversion

In the examples described in Fig. 8, we showed the good performance of the algorithm in reconstructing the ‘true’ anomaly. There, the quality of the match was estimated visually. But the real test of whether the approximation of the ‘true’ anomaly is satisfactory lies in whether it affects its interpretation (which is, ultimately, the reconstruction of its causative source). We test this via an inversion exercise.

Fig. 9a shows the same synthetic gravity profile used in previous tests. Fig. 9c shows its causative sources. Fig. 9b shows the profile with added noise (same amount as in previous tests). Fig. 9d shows the result of inverting the noisy profile. Here we assumed we know the causative sources have rectangular shape, and we inverted for their size, position and densities. Under this assumption the problem has a unique solution. We chose this approach since we wanted to avoid non-uniqueness confusing the evaluation of the algorithm performance. This is a simple inversion, and as expected the result closely matches the ‘true’ solution.

Fig. 9e shows the right hand side anomaly as reconstructed by the algorithm, while Fig. 9g shows the result of its inversion. Similarly Fig. 9h shows the result of inverting the left hand side anomaly (9f). It is quite clear from this example that the two isolated anomalies retained enough information to allow the correct reconstruction of the causative source, which is ultimately the purpose of any potential field analysis. Table 1 shows the exact parameters of the true sources and the numerical results of the three inversions.

In this simple example there is little benefit in separating the anomalies before inversion. In more complicated profiles however, there may be a considerably computational advantage in turning a single multi source inversion into several single source ones. Basically, this offers a way to deal with the ‘curse of dimensionality’ inherent in all inversion problems, by turning a high dimensional problem into several smaller dimensional ones.

Table I. Parameters defining the true sources (First row). Result of the inversion of the overall profile (second row). Result of the inversion of the individual anomalies (Third and fourth rows).

Left hand side source					Right hand side source					
	X1	X2	Z1	Z2	ρ	X1	X2	Z1	Z2	ρ
True Values	60	70	5	10	.25	140	190	5	10	.25
Inversion of overall profile	60.13	70.05	5.09	10.05	.2537	139.94	189.58	5.00	10.0	.2491
Inversion of left anomaly	59.68	70.44	5.39	10.36	0.24					
Inversion of right anomaly						139.93	189.64	5.04	10.0	0.2508

5.3 Signal processing

Moreau et al (1997) and Hornby et al (1999) have shown that wavelet analysis, and multiscale edge analysis in particular, is suitable for the analysis of potential field data. More recently, Holden et al (2001) and Poulet et al (2001) have shown that the location of the multiscales edges can be used to reconstruct the approximate location of causative sources in gravity inversion. Boschetti et al (2001) have shown that both location and amplitude of the multiscale edges can be used in conjunction with a

downward continuation process to reconstruct the depth-to-the-top of gravity sources, while Sailhac et al (2000) applied similar concepts to reconstruct the approximate representation of sources in magnetic surveys.

All these applications require information about the edges corresponding to a single anomaly at several scales (that is, at several different upward continuation heights). Depending on the horizontal separation between two anomalies, their signals will interfere at varying levels of upward continuation. When this happens, the position and amplitude of the multiscale edges will no longer carry information from one single anomaly (or *mostly* from a single anomaly) but, inevitably, about their superimposition. This is shown in Fig. 10. Fig. 10b shows a synthetic gravity profile. Fig. 10a shows its edge tree. At low scales (between 1 to 25 approximately) we can see 2 edges for each anomaly, as expected. After scale 40, approximately, we can no longer see 4 edges but only 2. Both anomalies have merged into a single one. Now the edges give information about the superimposition of the two anomalies. In between these two ranges, we have the transition zone which is usually very non-linear. In this example, we clearly can not use the full edge tree to infer the location and depth of the right hand side anomaly, since after scale 40 the edges contain information about the left hand side anomaly as well. Worse still, the edges of the left hand side anomaly are strongly distorted and die out after scale 30 approximately.

In order to circumvent the problem we can isolate the anomalies and reconstruct the correct edge trees. This is shown in Fig. 10c,d. Now all the edge-based algorithms mentioned above can be applied to both anomalies and the result will be minimally affected by the presence of the adjacent feature.

5.4 Application to Real Data

We conclude by showing the performance of the algorithm on a real data set. We selected a North South profile from the gravity map over Australia (see Fig. 11). The profile cuts perpendicularly to some very strong anomalies approximately in the center of the continent. Fig. 12a shows the profile we extracted. We want to isolate the part characterized by the strong signal variation. The result can be seen in Fig. 12b. Notice that, unlike all synthetic cases shown above, here the areas of the profile we want to remove are not characterized by a single clearly defined anomaly, but rather by an oscillating signal, with no clearly isolated feature. Nevertheless the algorithm worked successfully confirming again its robustness.

6 CONCLUSIONS

We propose two methods to isolate or remove anomalies from potential field data. One method, based on multiscale edge analysis, allows the removal of anomalies while leaving adjacent features basically untouched. The second method, based on iterative lateral continuation, accounts for the influence of adjacent features on one another. The choice of method depends upon the purpose of the analysis.

Ultimately, we envisage the use of the algorithms in conjunction with a visualisation package in which specific features can be selected and processed in real time, prior to further numerical inversion.

7 REFERENCES

Boschetti, F., Hornby, P. & Horowitz, F.G., 2001. Wavelet based inversion of gravity data, *Exploration Geophysics*, 32(1), 48-55.

Holden D., Archibald N., Boschetti F. & Jessell M., 2000. Inferring Geological Structures Using Wavelet-Based Multiscale Edge Analysis and Forward Models, *Exploration Geophysics*, 31(4), 617-621.

Hornby, P., Boschetti, F. & Horowitz, F., 1999. Analysis of potential field data in the wavelet domain, *Geophysical Journal International*, 137, 175-196

Jacobsen, B.H., 1987. A case for upward continuation as a standard separation filter for potential-field maps, *Geophysics*, 52, 1138-148.

Kaiser, G., 1994. *A Friendly Guide to Wavelets*, Boston, Birkhäuser.

Lu, J., Healy, D., & Weaver, J., 1994. Contrast enhancement of medical images using multiscale edge representation, *Optical Engineering*, 33, 2151-2161.

Lu, J., 1997. On consistent signal reconstruction from wavelet extrema representation, *Proc. of SPIE Wavelet applications in Signal and Image processing V, San Diego*, 14-25.

Mallat, S. & Zhong, S., 1992. Characterization of signals from multiscale edges, *IEEE Transaction on Pattern Recognition and Machine Intelligence*, 14, 710-32.

Mallat, S., 1998. *A wavelet tour of signal processing*, Academic Press, San Diego.

Moreau, F., Gibert, D., Holschneider, M. & Saracco, G., 1997. Wavelet analysis of potential fields. *Inverse Probl.*, 13, 165-178.

Poulet T., D'Escrivan H., Boschetti F., Hornby P. & Horowitz F., 2001. New Advances In The Analysis Of Potential Field Data By Multiscale Edges, *ASEG*, Brisbane, Sept 2001.

Sailhac P., Galdeano A., Gibert D., Moreau F. & et Delor C., 2000. Identification of sources of potential fields with the continuous wavelet transform: Complex wavelets and applications to magnetic profiles in French Guiana, *J. Geophys. Res.*, 105, 19455-19476.

FIGURE LEGENDS

Figure 1. Gravity profile containing 2 anomalies (top). The set of multiscale edges (middle). Profile reconstructed via MET (bottom).

Figure 2. Sketch of the MET. Notice that the full MET process goes through a standard wavelet transform.

Figure 3. (a) Synthetic gravity profile and its edge tree (b). (c) Edge tree after removal of the braches belong to the left hand side anomaly. (d) Right hand side anomaly after application of MET. (e) Difference between profile (a) and (d).

Figure 4. Description of the first step of the lateral continuation removal algorithm. (a) Original profile. (b) The right hand side anomaly is extrapolated laterally. (c) Profile in (b) is subtracted from the original profile leaving the first guess of the left hand side anomaly. (d) The left hand side anomaly is laterally extended to account for the edge values. (e) Profile in (d) is subtracted from the original profile, leaving the first guess of the right hand side anomaly.

Figure 5. (a) The gravity profile (dashed line) generated by the block source in (b). The left flank of the anomaly (dark line) is well approximated by a point source laterally displaced from the centroid of the block.

Figure 6. Location of the three points necessary to isolate the main anomaly.

Figure 7. (a) Original profile. (b) profile after removal of the left anomaly and (c) right hand side anomaly.

Figure 8. (a) Gravity profile to which a random white noise whose maximum amplitude is 15% of the signal amplitude was added (dashed), reconstructed signal (thick line) and ‘true’ signal (dotted). Even in the presence of heavy noise, reconstructed and true profile depart considerably only when the two anomaly are very close and interfere strongly.

Figure 9. (a) Synthetic gravity profile and (c) its causative sources. (b) profile with added noise. (d) result of inverting the noisy profile. (e) right hand side anomaly as reconstructed by the algorithm, and (g) result of its inversion. (f) left hand side anomaly as reconstructed by the algorithm, and (h) result of its inversion.

Figure 10. (b) Original profile and its edge tree (a). (d) right hand side anomaly and its edge tree (c). (f) left hand side anomaly and its edge tree (e).

Figure 11. Gravity map of the Australian continent. The white dashed lines represent the profile we extracted for analysis.

Figure 12. (a) Real gravity profile extracted from the gravity map over the Australia continent. The strong anomalies in the centre of the continent after being isolated (b).

TABLES

Table I. Parameters defining the true sources (First row). Result of the inversion of the overall profile (second row). Result of the inversion of the individual anomalies (Third and fourth rows).

Left hand side source					Right hand side source					
	X1	X2	Z1	Z2	ρ	X1	X2	Z1	Z2	ρ
True Values	60	70	5	10	.25	140	190	5	10	.25
Inversion of overall profile	60. 13	70. 05	5.0 9	10.05	.253 7	139. 94	189. 58	5.00	10.0 6	.249 1
Inversion of left anomaly	59. 68	70. 44	5.3 9	10.36	0.24					
Inversion of right anomaly						139. 93	189. 64	5.04	10.0 6	0.25 08

FIGURES

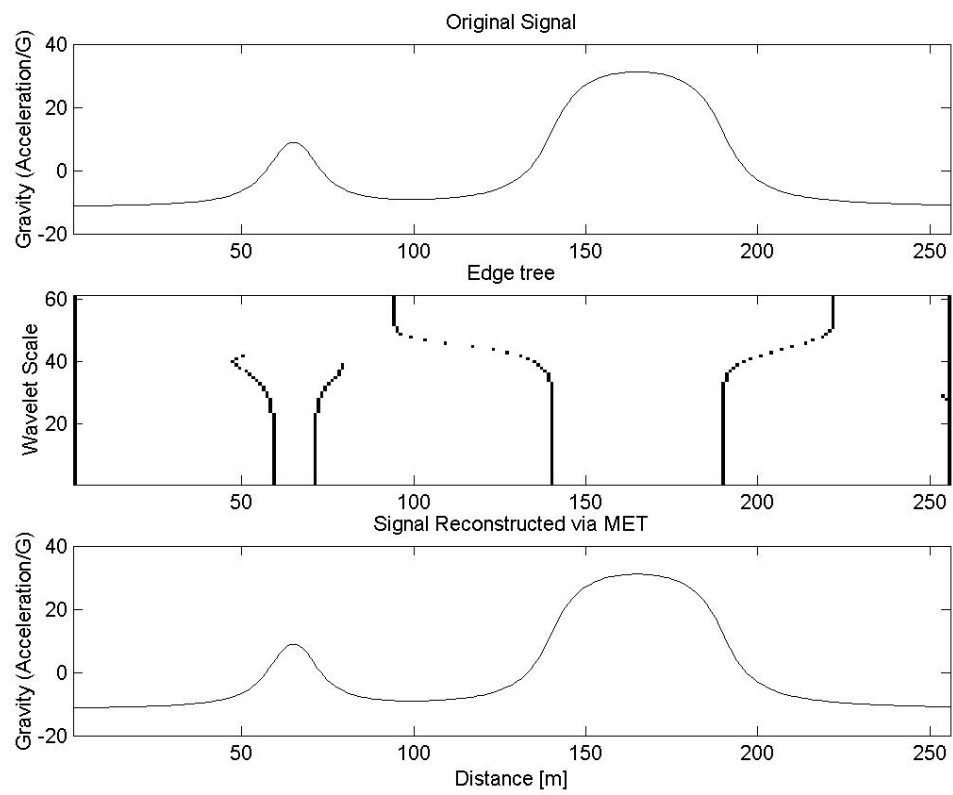


Figure 1

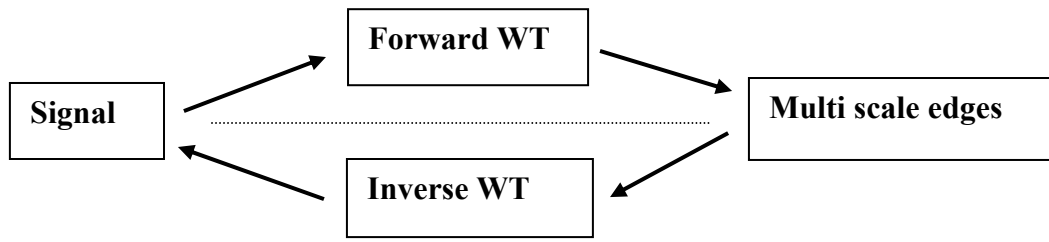


Figure 2

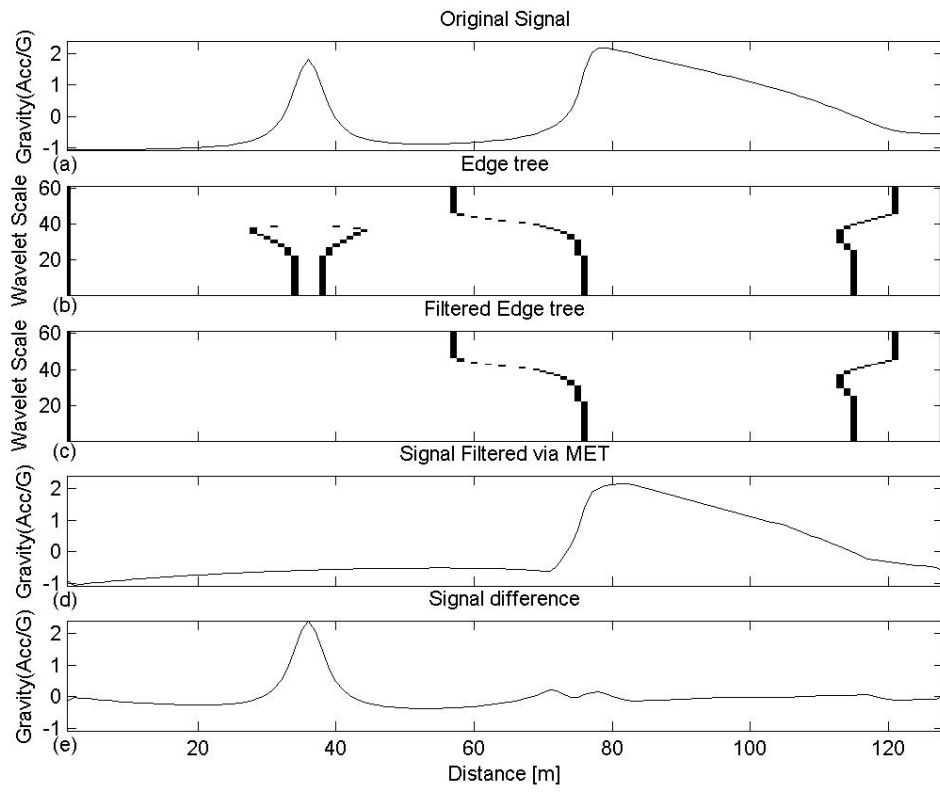


Figure 3

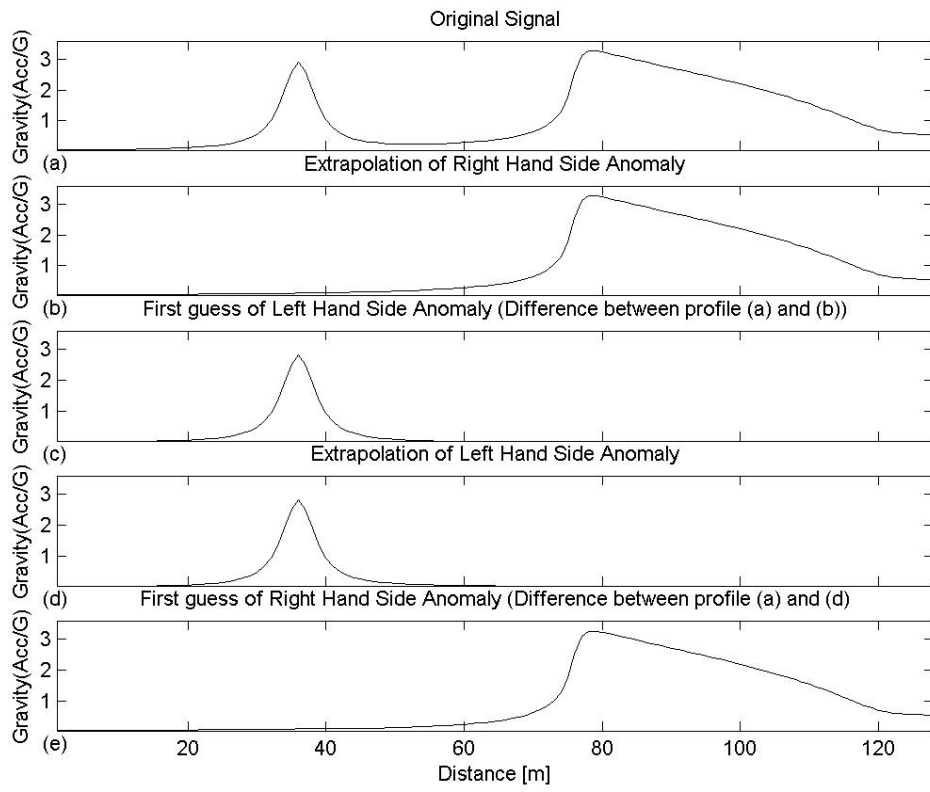


Figure 4

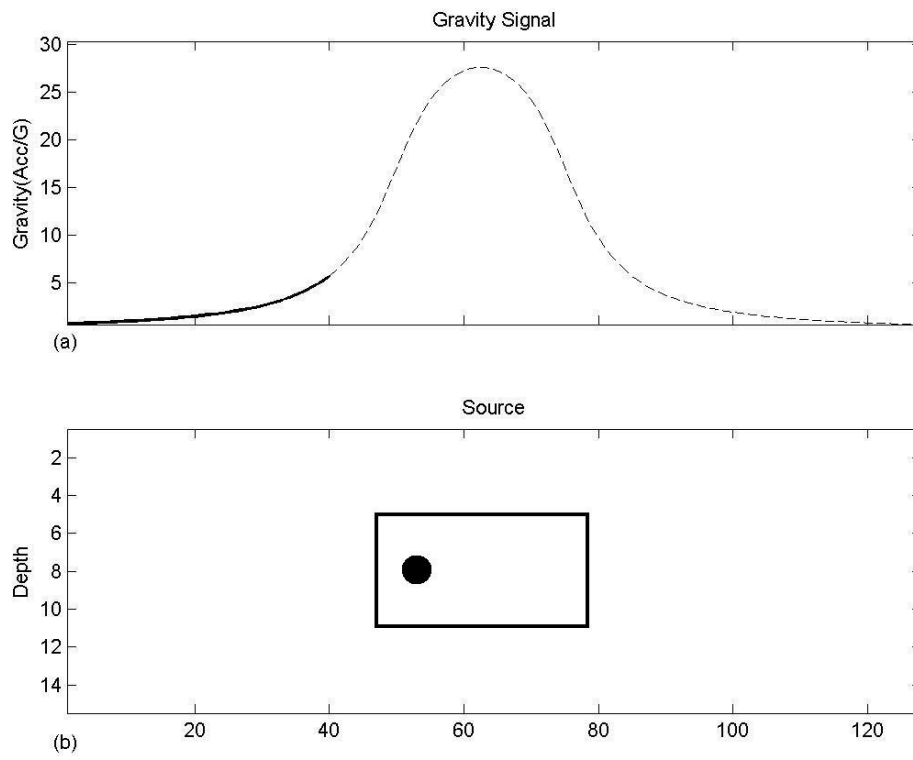


Figure 5

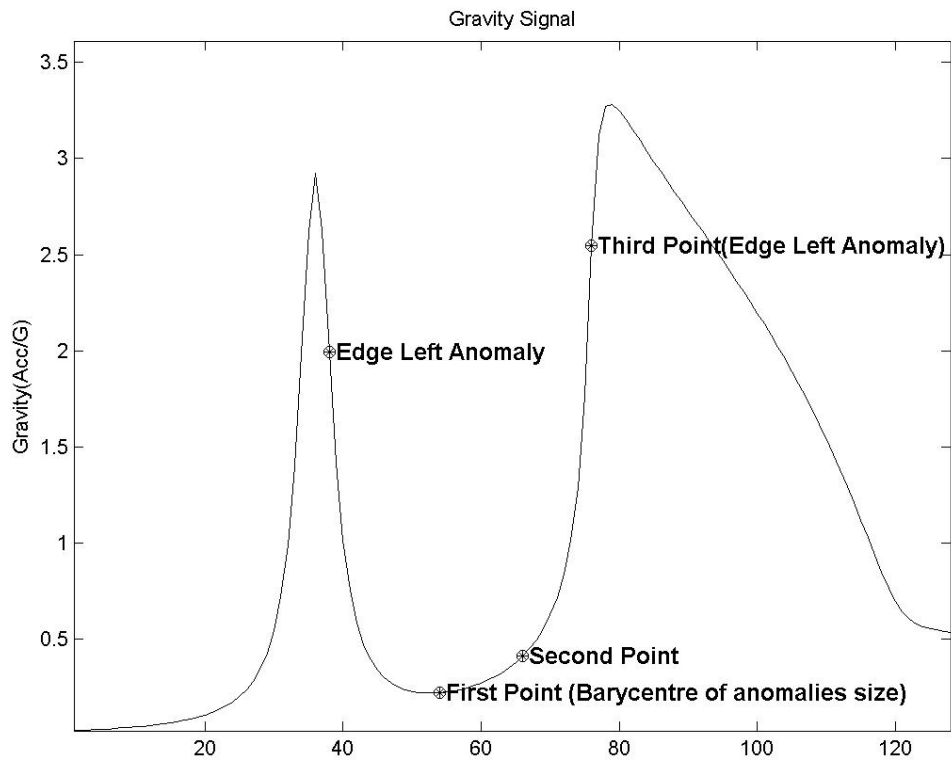


Figure 6

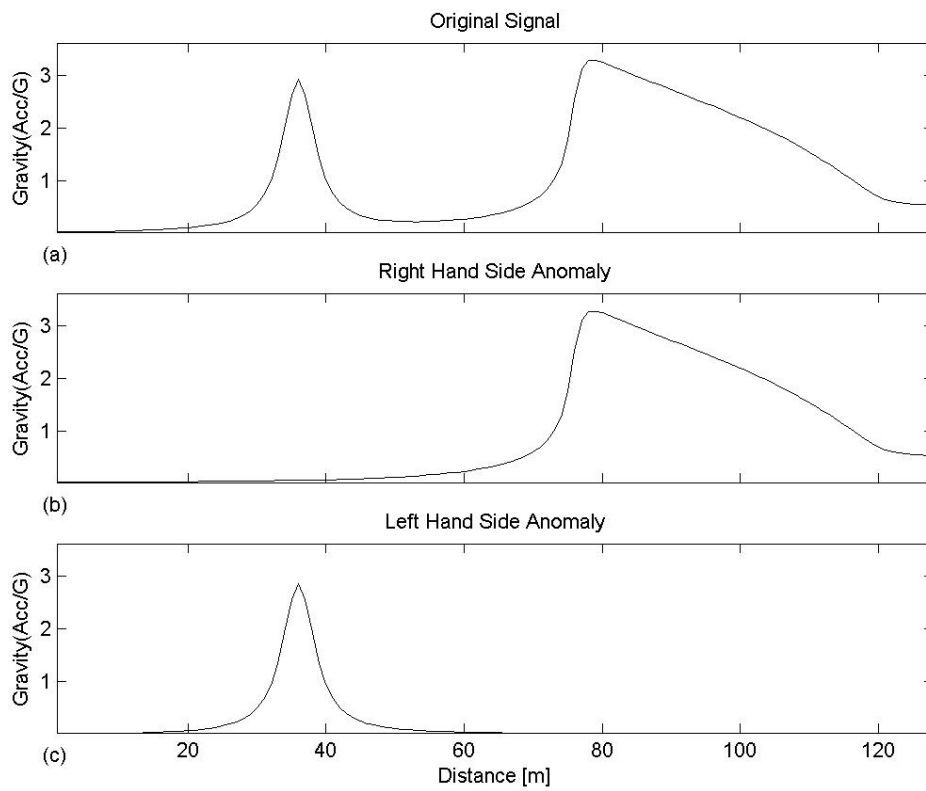


Figure 7

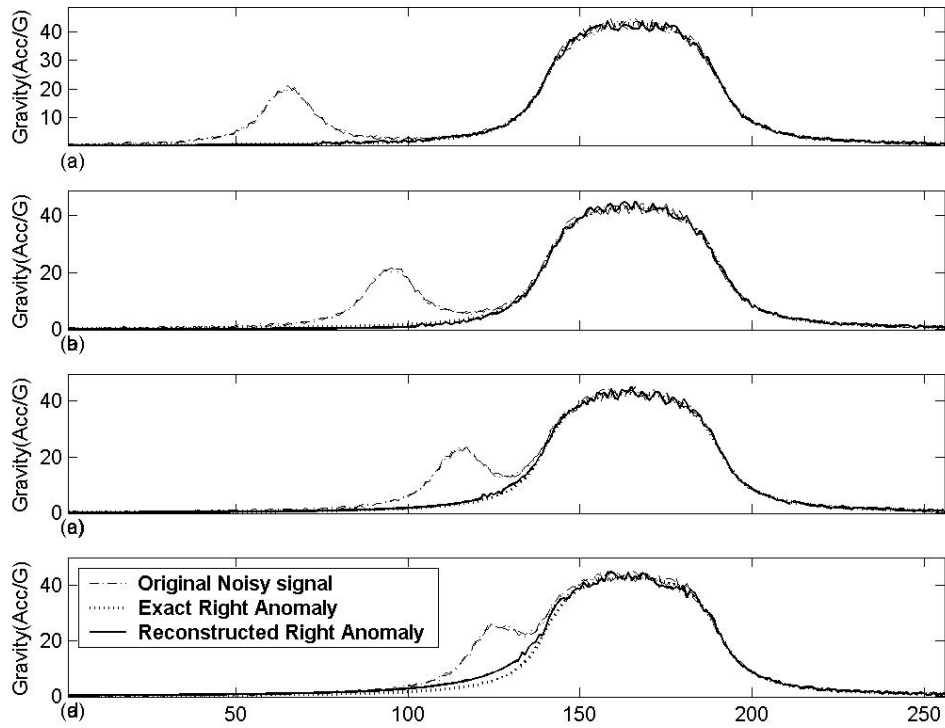


Figure 8

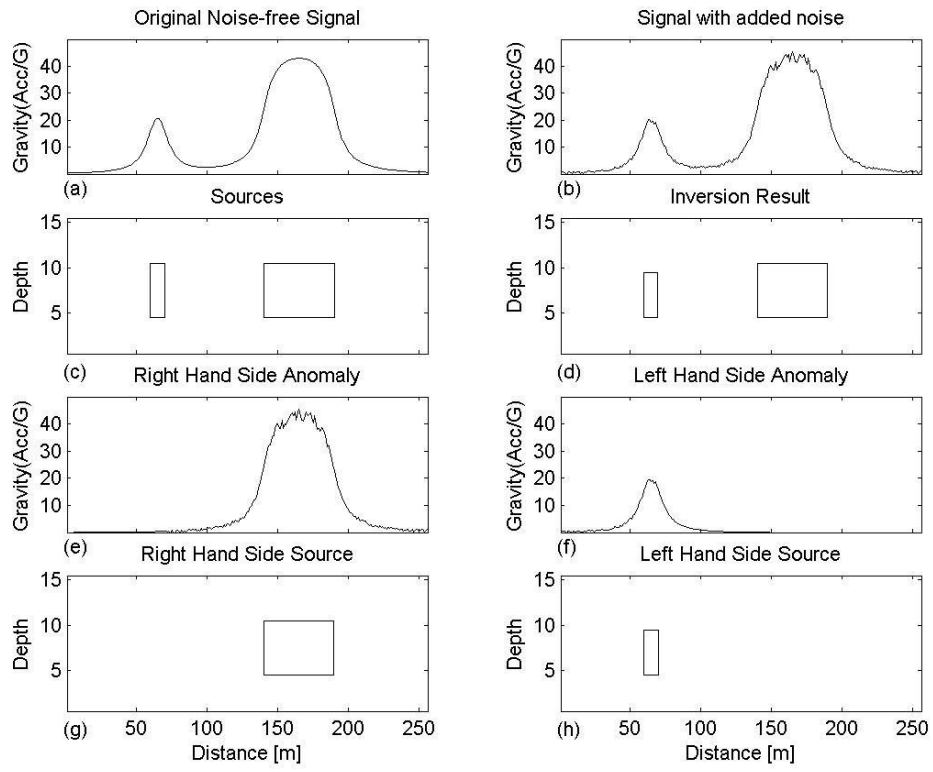


Figure 9

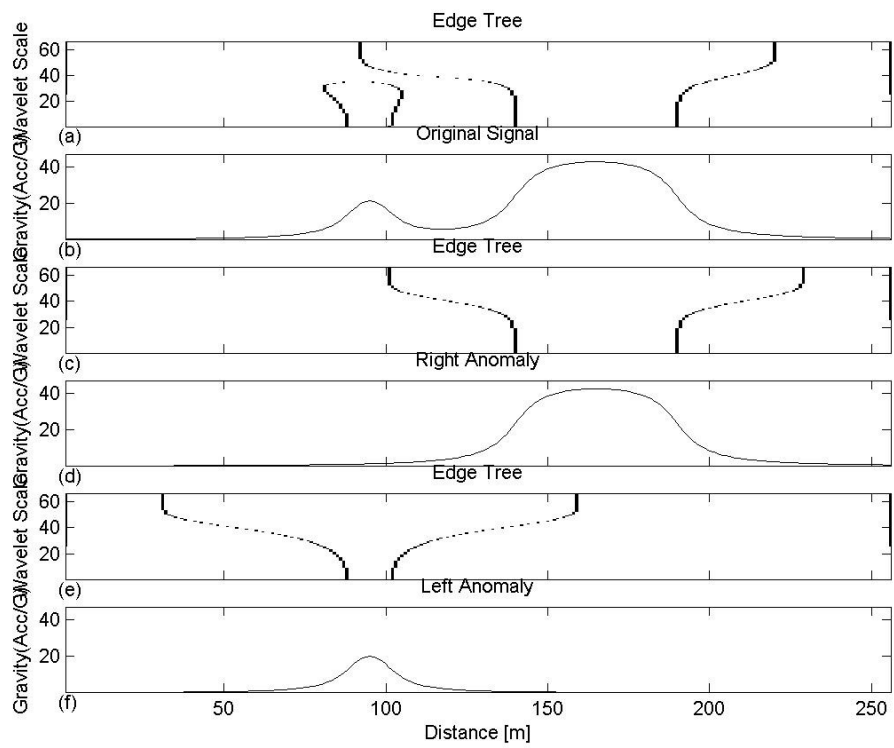


Figure 10

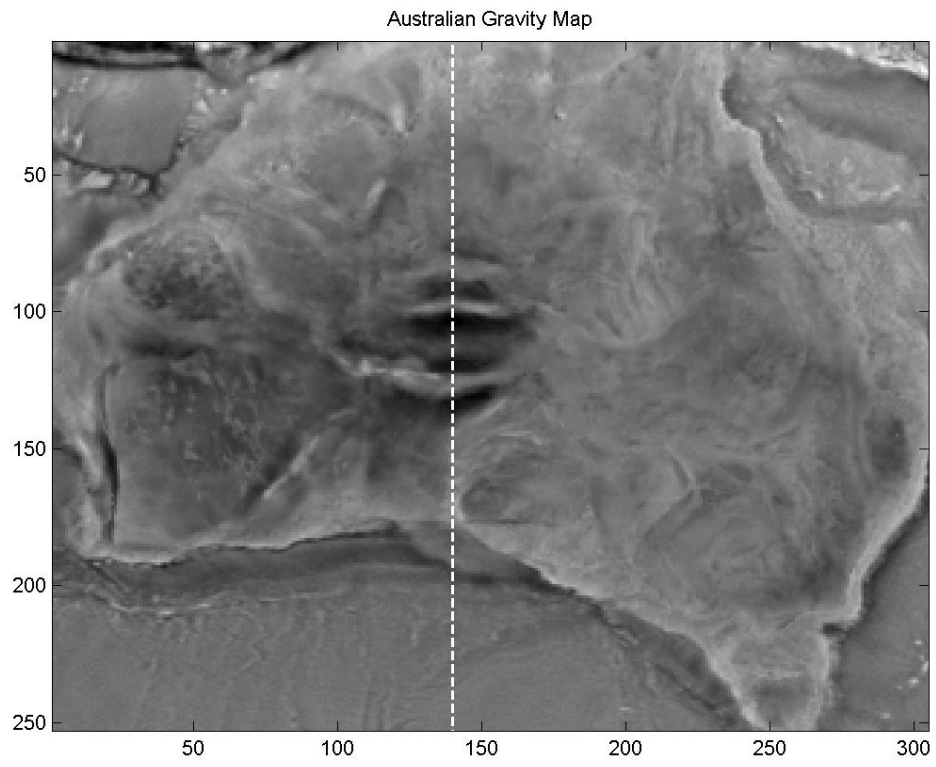


Figure 11

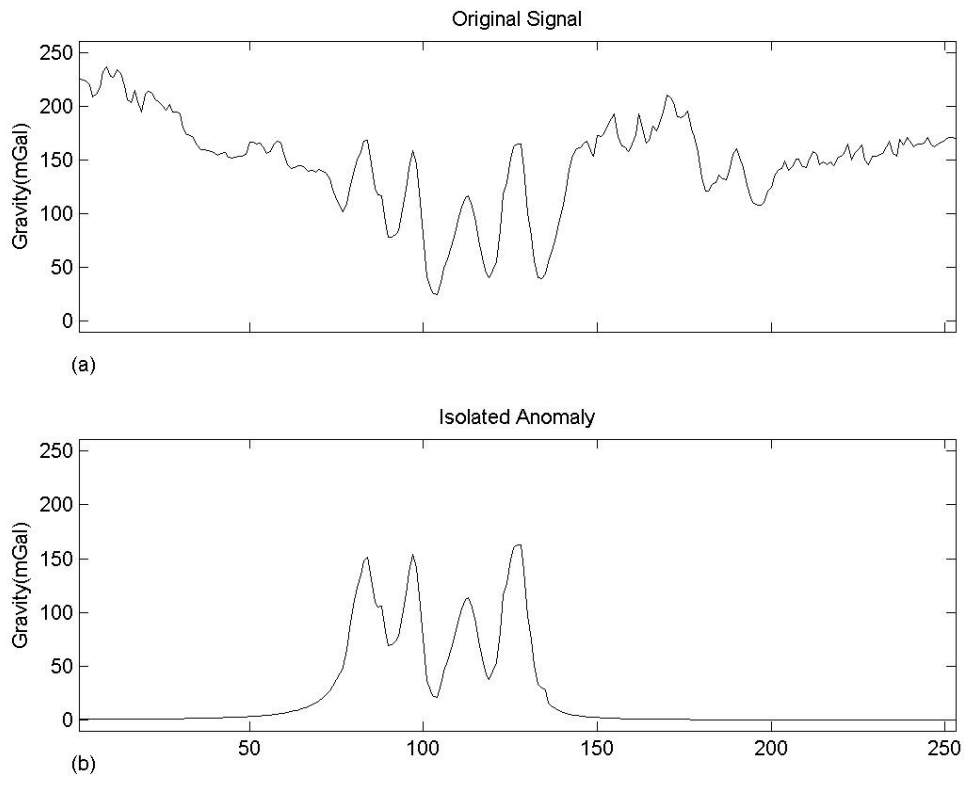


Figure 12